Beyond behavioural change

Investigating alternative explanations for shorter time headways when human drivers follow automated vehicles

Jiao, Yiru; Li, Guopeng; Calvert, Simeon C.; van Cranenburgh, Sander; van Lint, Hans

Beyond behavioural change: Investigating alternative explanations for shorter time headways when human drivers follow automated vehicles

Yiru Jiao [a,c,*], Guopeng Li [a], Simeon C. Calvert [a,c], Sander van Cranenburgh [b,c], Hans van Lint [a]

[a] Department of Transport & Planning, Delft University of Technology, Delft, The Netherlands
[b] Department of Engineering Systems and Services, Delft University of Technology, Delft, The Netherlands
[c] CityAI lab, Delft University of Technology, Delft, The Netherlands

ARTICLE INFO

ABSTRACT

Integrating Automated Vehicles (AVs) into existing traffic systems holds the promise of enhanced road safety, reduced congestion, and more sustainable travel. Effective integration of AVs requires understanding the interactions between AVs and Human-driving Vehicles (HVs), especially during the transition period in which AVs and HVs coexist in a mixed traffic environment. Numerous recent empirical studies find reduced headways of human drivers following an AV compared to following an HV, and attribute this reduction to behavioural changes of drivers when they follow AVs. However, more factors may be at play due to the inherent inconsistencies between the comparison conditions of HV-following-AV and HV-following-HV. This study scrutinises three alternative explanations for the observed reduction in headways: (1) systematic differences in car-following states during data collection, (2) systematic differences in driving variability between leading AVs and HVs, and (3) systematic differences in driving characteristics of leading AVs versus HVs. We use a large-scale dataset extracted from Lyft AV motion data and examine each of these explanations through data stratification and simulation. Our results show that all three mechanisms contribute to the observed reduction in headways of human drivers following AVs. In addition, our findings highlight the importance of driving homogeneity and stability in achieving reliably shorter headways. Thereby, this study offers a more comprehensive understanding on the difference between HV–AV and HV–HV interactions in mixed traffic, and is expected to promote more effective integration of AVs into human traffic.

1. Introduction

Automated vehicles (AVs) are expected to improve traffic conditions by enhancing road safety, reducing congestion, and allowing more accessible and sustainable travel (Litman, 2015; Meyer et al., 2017; Duarte and Ratti, 2018; Yao et al., 2020). Before achieving AV-dominated traffic, there may be a decades-long transition, during which AVs and human driving vehicles (HVs) coexist on the roads and form a mixed traffic environment (Calvert et al., 2017; Nikitas et al., 2019; Zheng et al., 2020). In this environment, AVs and HVs are required to interact with and adapt to each other.

Considerable attention has been paid to enabling AVs to interact with other road users and adapt to human-dominated traffic (Di and Shi, 2021; Mozaffari et al., 2022). In developing such socially compatible driving strategies for AVs, various approaches have been used to model and learn from social interactions between human drivers. In a comprehensive review of these endeavours (Wang et al., 2022), two key aspects are summarised. On the one hand, AVs need to understand and adapt to the social cues, intentions, and expectations of human drivers (Schieben et al., 2018; Liu et al., 2020; Xia et al., 2021). On the other hand, AVs also need to deliver informative social cues and recognisable interaction intentions so that human drivers can react accordingly to facilitate smooth and safe negotiations (Schwarting et al., 2019; Siebinga et al., 2022).

The way human drivers react to AVs is comparatively scantly explored. Existing empirical research predominantly focuses on car-following scenarios, and reports shorter distance and/or time headway of human drivers following AVs than following HVs. From field experiments, Rahmati et al. (2019) find a statistically significant difference in the behaviour of human drivers when following AVs versus HVs: human drivers tend to follow AVs more closely. Similar research by Mahdinia et al. (2021) and Zhang and Talebpour (2023) also notice a closer spacing when human drivers follow AVs compared to HVs. Additionally, the authors reveal less variation in speed and acceleration of human drivers following AVs, as well as larger values of minimum Time-to-Collision (TTC). These findings are reinforced by analyses based on data collected by Waymo's AV (Sun et al., 2020). Wen et al. (2022) corroborate that human drivers following AVs have shorter time headway, reduced variation in speed and acceleration, and increased TTC values. Based on the similar parameters of car-following behavioural modelling, Hu et al. (2023) argue for no significant behaviour difference between human drivers following AVs and those following HVs, except for shorter jam spacing. In line with previous studies, Wang et al. (2023) find that human drivers maintain smaller distances with AVs than HVs in the deceleration process when approaching traffic signals.

Distance headway and time headway are, respectively, spatial and temporal gaps between two consecutive vehicles – a leading vehicle and a following vehicle – in a traffic stream. For a following vehicle in motion, the distance headway from its leading vehicle equals the time headway multiplied by the following vehicle's speed. Although very small headways may imply dangerous situations (Vogel, 2003), shorter headways during car following are generally desirable from the perspective of macroscopic traffic efficiency (Makridis et al., 2020b). Maintaining shorter time headway allows more vehicles on the road, thereby potentially increasing road capacity and reducing traffic congestion (Schakel and van Arem, 2014; Bian et al., 2019).

The most common explanation for the reduced headways is that human drivers may change their behaviour due to different perceptions of the leading AVs (Hulse et al., 2018; Zhao et al., 2020). For example, human drivers may perceive increased comfort (Rahmati et al., 2019) or safety (Wang et al., 2023) when approaching AVs compared to HVs. Additionally, curiosity about AVs may prompt drivers to follow closely for observation or interaction (Hu et al., 2023). One of the primary anticipated advantages of autonomous driving, for improving traffic efficiency, is that AVs can reduce time headway from their leading vehicles (Aria et al., 2016; Yu et al., 2021; Aittoniemi, 2022). If human drivers tend to follow AVs at shorter headways, the potential benefits of integrating AVs into existing traffic could be significantly enhanced.

However, beyond the behavioural changes of human drivers following AVs, other factors such as imbalances in data collection and the way AVs drive can also play critical roles. Inconsistent conditions inherent in the HV-following-AV and HV-following-HV situations complicate an effective comparison of the headways between these two situations. For example, drivers are not asked to closely follow the vehicles preceding them in real-world road tests. The proportion of free-following states may thus be uneven in the data collected for human drivers following AVs and HVs. In addition, leading AVs share the same driving algorithms and tend to generate less varied contexts for their following vehicles. This contrasts with leading HVs that have a wide range of driving styles and create heterogeneous car-following contexts. Furthermore, AVs are operated by algorithms and can be precisely controlled, which may produce very different driving circumstances for their following vehicles, compared to HVs which are inevitably influenced by human factors. These inconsistencies, as a result, may induce statistical biases in headway observation and comparison.

For a more comprehensive understanding on the phenomenon of reduced headways when human drivers follow AVs, this study investigates alternative explanations other than human behavioural changes. We examine three underinvestigated factors: (1) the car-following states during data collection, (2) the driving variability of leading vehicles (i.e., the uniformity of AVs against the heterogeneity among HVs), and (3) the unique driving characteristics of AVs. Our examinations are based on a large-scale car-following dataset (Li et al., 2023) extracted from sensor data collected by Lyft AVs between October 2019 and March 2020 (Houston et al., 2021). For each factor, we isolate the factor by either stratifying the data or conducting controlled simulation experiments. After isolation, we evaluate each factor's impact by comparing the headway distributions of human drivers following AVs and HVs.

The rest of this paper is organised as follows. Section 2 describes the calculation of distance and time headway, and introduces the hypotheses to test for examining the three factors. Section 3 then explains the methodology for isolating each of the factors to test the hypotheses. In Section 4, we select the dataset to use and show a baseline headway reduction without isolating any factors. Then the effect of each factor on headway reduction when human drivers follow AVs is presented in Section 5. Finally, Section 6 concludes this paper and envisions future research. To improve readability and focus on the main findings, we place most of the direct experiment results in the appendices.

2. Conceptual framework

This section describes the conceptual structure of this study. We first explain the calculation of distance and time headway with data collected by automated vehicles (AVs), where we also point out the potential inconsistency in detection between human driving vehicles (HVs) following and passing by the AVs. Then we present the framework to examine 3 factors that may contribute to reduced headways when human drivers follow AVs compared to following HVs. Unlike commonly assumed behavioural changes of the following vehicle drivers, these factors are inherent in the data collection process and the attributes of the obtained data.
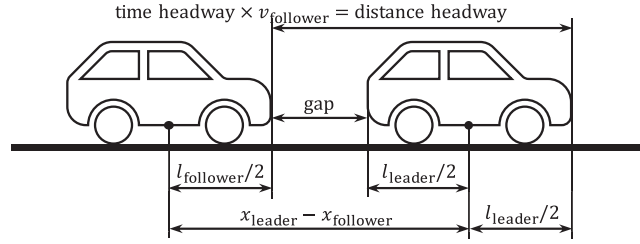
$$\text{time headway} \times v_{\text{follower}} = \text{distance headway}$$

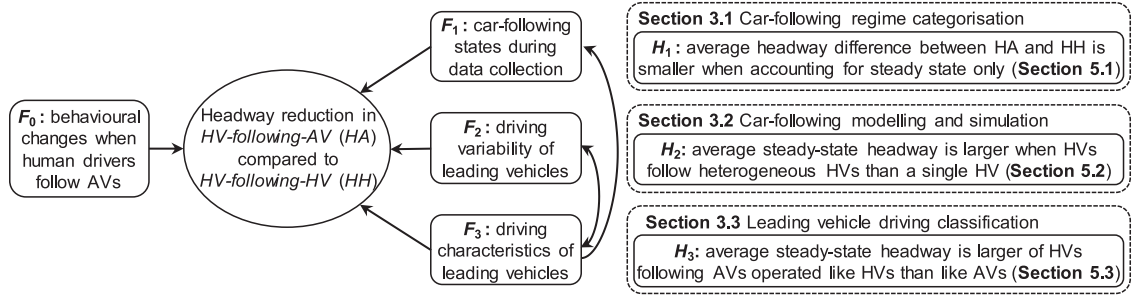**Fig. 1.** Calculation of gap, distance headway, and time headway with vehicle centroids.

Fig. 2. The analytical model of factors (F) and hypotheses (H) explored in this study.

2.1. Distance and time headway

Distance headway is the distance between the front bumpers of a leading vehicle and a following vehicle at the same time; time headway can be computed by dividing distance headway by the following vehicle's current speed. In traditional bird's eye view trajectory datasets such as NGSIM (Transportation – FHWA, 2008) and highD (Krajewski et al., 2018), vehicle positions are already assigned to the front bumpers. However, in the datasets collected by AVs, the positions of vehicles are given as the centroids of the 3D bounding boxes obtained in object detection using computer vision. The accuracy of these centroid positions is affected not only by the vision algorithms but also by the sensor placement. Especially during deceleration, this inaccuracy can increase significantly.

With centroid positions, the calculation of headways between vehicles requires vehicle length, as illustrated in Fig. 1. The leading vehicle is denoted by the subscript $_{\text{leader}}$ and the following vehicle by $_{\text{follower}}$. Their positions, speeds, and vehicle lengths are correspondingly denoted as x, v, and l. In AV-collected data, the lengths of HVs are processed based on the AV's detection results. According to Qian et al. (2022), 3D object detection from LiDAR and camera data makes errors primarily regarding vehicle dimensions. This can be caused by occlusion of the AV per se or of other surrounding vehicles, especially for detecting vehicles when they do not move. Therefore, HVs following HVs and passing by an AV are generally more visible to the AV's sensors, whereas HVs that follow directly behind the AV are more probable to be unreliably detected.

The headways to be compared need to be reliable. We assume that the length distributions of HVs following AVs and of HVs following HVs are similar. If the detected lengths of HVs following AVs align with the detected lengths of HVs following HVs, the detection of vehicle lengths can be considered reliable. Then we will calculate and compare both distance headway (DHW) and time headway (THW) in Eq. (1). Otherwise, given that time headway is less biased by vehicle lengths, our comparison will use Eq. (2) and consider time headway only.

$$\begin{cases} \text{DHW} = x_{\text{leader}} - x_{\text{follower}} - l_{\text{follower}}/2 + l_{\text{leader}}/2 \\ \text{THW} = \text{DHW}/v_{\text{follower}} \end{cases} \tag{1}$$

$$\text{THW} = (x_{\text{leader}} - x_{\text{follower}})/v_{\text{follower}} \tag{2}$$

2.2. Factors and hypotheses to be examined

Fig. 2 depicts our analytical model to explore alternative factors (abbreviated as F) beyond human behavioural changes (F_0) to explain the headway reduction when human drivers follow AVs. These factors can affect each other. To isolate each of them and accurately assess their individual impact, we use different methods, the details of which will be provided in Section 3. Based on the methods, we make hypotheses (abbreviated as H) to be tested in Section 5. These factors and hypotheses will be detailed in the next paragraphs.
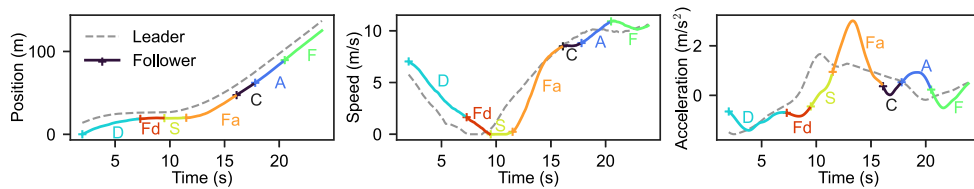
Fig. 3. An example of car-following regimes in urban traffic.

The first factor we consider is the car-following states during data collection, which can be influenced by traffic conditions, road layouts, and the driving characteristics of leading vehicles. Vehicles have varying headways in different car-following states such as free-following, accelerating, and decelerating. When car-following states are unevenly distributed in the data collected for HV-following-AV (HA) cases and HV-following-HV (HH) cases, comparing the statistics of headways in both cases will be biased. To address this imbalance, we categorise car-following states, based on which we can stratify the data and compare headways following AVs and HVs in the same condition. If the average difference in headway between HA and HH cases is less significant when only steady-state following is considered, we can tell the effect of the first factor.

The second factor is the driving variability of leading vehicles, more specifically, the uniformity of AV driving versus the heterogeneity of human driving. Different human drivers may behave differently in identical car-following states, while AVs tend to maintain consistent reactions due to programmed behaviours. Consequently, leading HVs can generate heterogeneous car-following contexts, while leading AVs maintain more uniform patterns. This difference is then further transmitted to the variability difference of the following HVs, of which higher heterogeneity leads to a broader distribution of headways (Li and Chen, 2017; Makridis et al., 2020a). To examine the impact of leading vehicle driving variability, we first calibrate car-following models and then conduct controlled simulation experiments using the calibrated models. Both the calibration and simulation are performed with HH cases only to control for the driving characteristics of leading vehicles. If the average headway during steady-state following is larger when the same HVs follow heterogeneous HVs than following a single HV, we can validate the impact of the second factor.

The third factor we consider is the driving characteristics of leading vehicles, which is distinct of AVs from HVs. AV driving is controlled by precise, prescriptive, and fast-responding algorithms, whereas human driving is often uncertain, unpredictable, and has varying reaction time (Shi and Li, 2021). This distinction may result in different headways of drivers following AVs and HVs. To distinguish between the driving characteristics of leading AVs and HVs, we first train a neural network using half of the trajectories in HA and HH cases. Then we apply the trained network to the other half of the trajectories to identify HV-like and AV-like driving dynamics of AVs. Assessing the third factor's impact while controlling for the driving variability of leading vehicles then can be achieved by answering the question: will human drivers have longer headways when following an AV that resembles human driving than following an AV that drives less like HV? If so, the effect of the driving characteristics of AVs on headway reduction can be validated.

3. Methodology

To rigorously isolate the factors and assess their impacts, we utilise a variety of methods. As presented in Section 3.1, we distinguish different car-following states using a car-following regime categorisation algorithm. This enables comparing headways in similar conditions across following automated vehicles (AVs) and human driving vehicles (HVs). Section 3.2 deals with the driving variability of leading vehicles. We calibrate car-following models to simulate the behaviour of human drivers, and then have the same set of models follow two separate groups of leading vehicles with higher and lower driving variability. Finally, we train a neural network to classify whether a leading vehicle's driving behaviour is more characteristic of an AV or an HV, as detailed in Section 3.3. This allows for evaluating the influence of AVs' driving characteristics.

3.1. Isolation of car-following states — car-following regime categorisation

Car-following consists of longitudinal interactions between leading vehicles (leaders) and following vehicles (followers) under various traffic conditions. In this context, a car-following regime refers to a driving situation experienced by the follower (usually constrained by the leader). In highway traffic, Treiber and Kesting (2013b) categorise 5 car-following regimes as cruising at a desired speed (C), accelerating following a leader (A), decelerating following a leader (D), constant speed following (F), and staying stationary (S). Decelerating and temporary stopping in free-flow are excluded because the traffic flow on highways is highly continuous. However, car-following faces more interruptions in urban environments, such as vulnerable road agents (e.g., cyclists and pedestrians) and traffic signals. Therefore, in this study, we consider two additional regimes: free accelerating less constrained by a leader (Fa), and free decelerating less constrained by a leader (Fd).

For a more intuitive understanding, we present a real example of these car-following regimes in Fig. 3. In the regimes of C, Fa, and Fd, the time series of speed and acceleration of the follower are more independent of the leader's, as the follower's behaviour is less constrained by the leader. In contrast, in the regimes of F, A, and D, the follower is more constrained by the leader, and the follower's behaviour resembles the leader's after a certain delay of reaction. The regime S can happen after the regime Fd or D.

We adapt the algorithm proposed by Sharma et al. (2018) to categorise the car-following regimes in each case based on the trajectories of the leader and the follower. The algorithm consists of three steps:

(1) dividing the follower's speed profile into various segments,
(2) distinguishing the divided segments between car-following and free-following, and
(3) determining the regime for each divided segment based on the acceleration within it.

In the second step, the distinguishing thresholds in HA cases and HH cases are respectively selected based on the mean value and standard deviation of the time gap distribution of each, where the time gap for every case is calibrated from Newell's car-following model (Newell, 2002). Appendix A.1 shows these steps in more algorithmic detail. For further investigation, we refer the reader to Sharma et al. (2018).

3.2. Isolation of driving variability — car-following modelling and simulation

Car-following models describe the dynamics of a following vehicle adapting the speed and maintaining a safe distance from its leading vehicle, ranging from theory-based kinematic models, psycho-physical models, to data-driven models (a detailed survey is referred to Zhang et al., 2023). These models, to various degrees, may not capture the complete complexity of human driving behaviour (Hamdar, 2012). Here our focus is on evaluating the contribution of driving variability to headway distribution differences. This requires different combinations of model parameters to simulate the heterogeneous car-following behaviour of drivers. For this purpose, we select the widely used Intelligent Driver Model (Treiber et al., 2000) here, and we also provide the option of using Gipps' model (Gipps, 1981) in the Appendix A.4.

3.2.1. Intelligent driver model and its calibration

As defined in Eq. (3), the Intelligent Driver Model (IDM) uses a continuous nonlinear function $f : \mathbb{R}_{>0}^2 \times \mathbb{R} \mapsto \mathbb{R}$ to produce the acceleration profile of a follower based on its own speed (v), the relative speed of the follower and the leader (Δv), and the distance between them (s). The s is typically interpreted as the net distance, i.e., the gap, between the leading and following vehicles on highways. Whereas in urban traffic, vehicle gaps can be considerably small and lead to acceleration fluctuations and negative speeds in simulating standstills. To mitigate this issue, we consider s as the distance headway between vehicles, so that the minimum value of s must be greater than the length of the leading vehicle.

$$
\dot{v} = f(v, \Delta v, s) \triangleq \alpha \left[1 - \left(\frac{v}{v_0} \right)^{\delta} - \left(\frac{s^*(v, \Delta v)}{s} \right)^2 \right]
$$
$$
s^*(v, \Delta v) = s_0 + \max \left(0, vT + \frac{v \Delta v}{2\sqrt{\alpha \beta}} \right)
$$

(3)

The IDM parameters correspond to different behaviours during car following. v_0 is the desired speed when the follower is freely running without reaction to the leader; s_0 is the minimum distance headway and indicates the desired distance from the leader when both the follower and the leader are stationary; T, in parallel, indicates the desired time interval between them. Therefore, $s_0 + vT$ is a safe distance for followers at a speed of v to keep from their leaders. When the follower approaches a slower or stopped leading vehicle, the IDM assumes that the deceleration usually does not exceed a comfortable deceleration β. A maximum acceleration α is reached when the follower freely accelerates from a standstill. With increasing speed, the vehicle's acceleration decreases, and goes to zero when the speed approaches v_0. This reduction is controlled by the exponent δ.

Eq. (3) may still result in negative speeds when the following vehicle stops or slowly approaches its leading vehicle in a distance smaller than s_0. Such negative speeds can jeopardise model calibration[1] and may cause further problems in simulation. This effect is particularly notable in urban traffic, where red lights at signalised intersections and pedestrians frequently stop vehicles. We thus use Eq. (4) to remedy Eq. (3).

$$
\dot{v} = \begin{cases} 0, & \text{if } v \leq 0 \wedge s < s_0 \\ f(v, \Delta v, s), & \text{otherwise} \end{cases}
$$

(4)

Eq. (4) defines discontinuous acceleration and requires the input data to satisfy that (1) the speed of the leading vehicle is non-negative at any time; (2) the speed of the leading vehicle is zero only at a finite number of time steps; (3) the initial speed of the following vehicle should be non-negative; (4) the initial gap between the leading and following vehicles should be larger than zero. As proved by Albeaik et al. (2022), these requirements ensure that a unique set of IDM parameters exists for any car-following horizon within finite time.

For the purpose of simulation, we calibrate IDMs based on evolving predictions of the follower's trajectories. Given the leader's trajectories and the follower's initial state, the accelerations, speeds, and positions of the follower are iteratively predicted at each time step based on the prediction at the previous time step. Under this approach, a suitable objective function for calibration is set according to Treiber and Kesting (2013a) as shown in Eq. (5), where $v = 0$ is not counted in.

$$
\underset{v_0, s_0, T, \alpha, \beta}{\arg\min} \frac{\sum(\hat{v} - v)^2 / |v|}{\sum |v|} + \frac{\sum(\hat{x} - x)^2 / |x|}{\sum |x|}
$$

(5)

---

[1] Negative speeds can prevent model calibration when δ is not an even number; when δ is an even number, negative speeds can lead to larger deceleration and reinforce the negative speeds, making the modelled dynamics deviated.

Table 1
Design of simulation experiments for examining the effect of leading vehicle variability on headways.

Variability	Number of leader(s)	Number of followers	Note
Uniform	1	$N_{HH} - 1$	Conducted 4 times with 4 different leaders,
Heterogeneous	$N_{HH} - 1$	$N_{HH} - 1$	and no followers follow their factual leaders

To obtain valid parameters and representative IDMs, the input trajectories for calibration should include sufficient driving regimes (Treiber and Kesting, 2013b; Sharma et al., 2019). According to Sharma et al. (2019), a minimum inclusion of 3 key regimes – A, D, and F – is essential; additional inclusion of regimes C, Fa, and/or S can further enhance the calibration robustness. Due to frequent disruptions in urban traffic, the regime C identified by the method in Section 3.1 is not necessarily at a desired speed, but simply signifies cruising at a certain speed. Therefore, the eligible car-following cases for calibration should have a maximum follower speed larger than 10 m/s (rather than the cruising regime C) and contain at least 0.5 s of each of the regimes of A, D, F, and either Fa or S.

3.2.2. Controlled simulation experiments

With the calibrated car-following models, we can simulate a variety of car-following cases under designed conditions. In each simulated car-following case, the follower's behaviour is described by a set of model parameters; the leader's behaviour and the initial state of its follower inherit the original trajectories of a factual case; then we simulate how the follower maintains speed and spacing from the leader. At each time step, we compute the current acceleration for the follower as $\dot{v}$ by using Eqs. (3) and (4). Denoting the computed acceleration $\dot{v}$ as $\hat{a}$, the speed derived from $\hat{a}$ as $\hat{v}$, and the reproduced position as $\hat{x}$, we update the follower's speed and position profiles as follows:

$$
\begin{cases}
\hat{v}^{(t+\Delta t)} = \max\{0, v^{(t)} + \hat{a}^{(t)}\Delta t\}, \\
\hat{x}^{(t+\Delta t)} = x^{(t)} + \frac{v^{(t)} + \hat{v}^{(t+\Delta t)}}{2}\Delta t.
\end{cases} \tag{6}
$$

To facilitate model calibration and based on the fact that people's reaction time to visual-acoustic stimuli has an average of 0.3 s (Teramoto et al., 2017; Carlsen et al., 2020), we set $\Delta t = 0.3$ s as the decision interval in simulation.

We design two groups of simulations to examine the variability of leader driving. In order to control for the potential impact of AVs' driving characteristics, the simulations use car-following trajectories and calibrated IDMs only of HH cases where both leading and following vehicles are human-driven. Table 1 shows our design with N_{HH} eligible HH cases.

These simulations are designed to contrast between following a single leader and many heterogeneous leaders. The single leader represents uniform leader driving; while the other $N_{HH} - 1$ leaders represent heterogeneous leader driving. Then we let the same $N_{HH} - 1$ HV followers follow the two sets of leaders. The single leader is selected from eligible HH cases with the largest time proportion of regimes F and S, to ensure that steady-state headways are observed. We also make sure that no followers follow their factual leaders in the randomly paired simulations, to avoid introducing or enhancing the headway patterns obtained from IDM calibrations. In addition, we conduct the experiments for 4 times, each with a different uniform leader, to have a more robust comparison.

3.3. Isolation of driving characteristics — leading vehicle driving classification

In order to differentiate whether a leading vehicle drives more like an AV or HV, we design a neural network classifier. The classifier is composed of a recurrent neural network (RNN) encoder and a linear decoder followed by a function that normalises the output to (0,1). The encoder is a two-layer long short-term memory (LSTM) RNN (Hochreiter and Schmidhuber, 1997; Sak et al., 2014) for receiving and processing the input trajectories. LSTM is particularly well-suited to time series data, designed to handle the information evolving over time. Then the decoder is simply a layer of fully-connected network, which compresses the hidden states of the last layer of LSTM into a single number. Finally, we use the sigmoid function to convert that number into a probability between 0 and 1.

We use the binary cross-entropy (BCE) as the loss function between the ground truth labels and the predictions made by the classifier. As shown in Eq. (7), y_i is the ground truth label, p_i is the model's predicted probability for the ith sample, and N is the number of samples being evaluated. We emphasise that the accuracy of this classifier should not be extremely high, since some situations are in fact fuzzy to determine whether they are obtained from AV driving or HV driving. More importantly, in order to assess the effect of AV's driving characteristics on headways, our objective is to utilise the classifier to identify driving situations that are operated by AVs but are classified as by HVs.

$$
\text{BCE loss} = -\frac{1}{N}\sum_{i=1}^{N}\left[y_i \cdot \log(p_i) + (1 - y_i) \cdot \log(1 - p_i)\right] \tag{7}
$$

We frame the training material as a 148×2 tensor consisting of two movement variables over 14.8 s. These two variables are speed and acceleration, in order to reflect the driving dynamics of a leading vehicle. Although speed and acceleration are interrelated to each other, neither of them can be used alone because they each bear unique information that evolves over time.

In the original data, the duration of each car-following case varies from less than 15 s to more than 5 min. For the convenience of applying the model, we extract continuous segments for 14.8 s as sub-cases (since the shortest duration in HA cases is 14.8 s). Thus the cases shorter than 14.8 s are excluded, and each case that is longer than 14.8 s is separated into multiple (at least two) sub-cases. We also exclude the cases with a standstill period longer than 14.8 s, to avoid any sub-cases being completely stationary and indistinguishable.

Three data sets for model training, model validation, and model performance test, are then prepared. Considering that the average duration of HA cases is longer than that of HH cases, we first divide the HA cases into two groups of equal number, and then randomly select HH cases with a number 1.094 times the number of HA cases (HA cases are generally longer than HH cases, this is to ensure a similar number of sub-cases), also in two groups. The leaders in the first divided HA group and HH group are combined and used as the training set. The leaders in the combination of the other HA group and HH group form the validation set. Then we use the leaders in all AV-following-HV cases as an out-of-distribution test set of leading HVs. We label HV leaders as 0 and AV leaders as 1. Therefore, both the training set and validation set contain half HV leaders (labelled 0) and half AV leaders (labelled 1), and the test set consists of all HV leaders (labelled 0).

After the training, we apply the classifier to the segmented sub-cases in the validation set. To counteract the previous segmentation of car-following, we need to aggregate the obtained predictions corresponding to their original time steps and cases. In this way, our analysis can still be based on the complete car-following cases. Therefore, we define two types of aggregation as shown in Eq. (8), where p_i is the prediction of a sub-case i. The sub-case i belongs to case c_i and the time steps covered by i are denoted by t_i.

$$
\begin{cases}
p_c = \dfrac{1}{N_c} \displaystyle\sum_{\{i \mid c_i = c\}} p_i, & \text{for each case } c \\[4mm]
p_c^{(t)} = \dfrac{1}{N_t} \displaystyle\sum_{\{i \mid t \in t_i \text{ and } c_i = c\}} p_i, & \text{for each time step } t \text{ in a case } c
\end{cases}
\tag{8}
$$

If $p_c < 0.5$, the case c is classified to be more probable to have an HV leader; if $p_c > 0.5$, an AV leader is classified to be more probable. Similarly, if $p_c^{(t)} < 0.5$, the driving dynamics at time t in case c is more probable to be operated by an HV; if $p_c^{(t)} > 0.5$, the operation is classified to be more characteristic of an AV.

4. Data

This study investigates potential explanations for the reduced headways when human drivers follow automated vehicles (AVs) compared to human driving vehicles (HVs). For a comprehensive view, large-scale and real-world data recording the behaviour of both AVs and HVs is necessary. In recent years, numerous AV companies have released motion datasets collected through LiDARs and cameras equipped on their AVs (e.g., Chang et al., 2019; Caesar et al., 2020; Sun et al., 2020; Houston et al., 2021; Malinin et al., 2022; Wilson et al., 2023). These datasets provide valuable opportunities for studying human adaption of AVs, but also pose unique challenges for behaviour analysis due to the way the data are collected. Data collection by AVs takes a similar perspective to that by instrumented probe vehicles, as moving observers. It makes high-quality data available for microscopic traffic analyses (Coifman et al., 2016; van Erp et al., 2018); however, different from drone-collected data such as highD (Krajewski et al., 2018) and pNEUMA (Barmpounakis and Geroliminis, 2020), may have inconsistent detection errors for road users in different surroundings.

With these challenges in consideration, Section 4.1 first selects a suitable dataset for the current study and Section 4.2 gives an overview of the vehicle dynamics in the selected dataset. Next, based on the strategy described in Section 2.1, we show in Section 4.3 that the detection of HV lengths by AVs is biased. Therefore, we compare time headway only hereafter, and present a baseline of time headway reduction in Section 4.4.

4.1. Dataset selection

Among the AV-collected datasets, there are two specifically processed and open-sourced for studying car-following behaviour. One (Hu et al., 2022) is extracted from Waymo open data (Sun et al., 2020), and the other (Li et al., 2023) is extracted from Lyft open data (Houston et al., 2021). In the extracted datasets, movement dynamics of the vehicles are recorded at a frequency of 10 per second and are carefully filtered and denoised. Further, large vehicles such as buses and heavy trucks are excluded for a focus on the comparable behaviours of passenger cars.

Table 2 compares the two car-following datasets extracted from Waymo and Lyft open data. The collection of Waymo data was in multiple cities in the U.S. (i.e., San Francisco, Phoenix, and Mountain View) prior to its initial release in August 2019. In contrast, the Lyft data was collected between October 2019 and March 2020 by 20 automated vehicles along a fixed route in Palo Alto, California. Both datasets organise data as vehicle trajectories in various car-following cases. Each case is composed of two vehicles, where one continuously runs directly behind the other. There are hence three categories of car-following cases: AV-following-HV (AH), HV-following-AV (HA), and HV-following-HV (HH).

For investigating the reduced headways of human drivers following AVs, our analyses are majorly on HA and HH cases. Particularly, in order to evaluate the impact of driving variability as described in Section 3.2, two requirements need to be fulfilled. First, the follower in each case should have stationary moments for estimating a minimum acceptable gap. Second, the follower in

Table 2

Comparison of Waymo and Lyft car-following datasets.

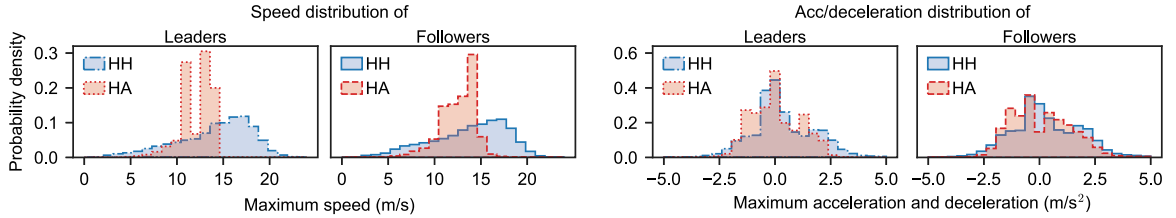| Data source	Collection time	Category	Number of cases	Number of valid cases	Average duration of valid cases (s)
Waymo	Before Aug. 2019	AH	210	27	19.75
		HA	286	33	19.76
		HH	1117	135	19.54
Lyft	Oct. 2019–Mar. 2020	AH	9,172	1,886	24.86
		HA	29,449	5,542	38.92
		HH	42,892	9,243	21.65

Fig. 4. Distributions of vehicle dynamics in HH and HA cases.

each case should reach a high enough speed to be considered as the desired speed. Accordingly, we select valid cases where the minimum speeds of both the leader and follower are smaller than 0.1 m/s, and the maximum speeds of the follower exceed 10 m/s. A larger average duration of these valid cases then implies a wider range of driving dynamics. As shown in Table 2, the dataset extracted from Lyft data has notably more valid cases and longer average duration across all three categories of car-following cases. As such, the Lyft car-following dataset can provide better support for our analyses, and is thus used in this study.

4.2. Vehicle dynamics overview

The Lyft open data was collected during daytime hours between 8 a.m. and 4 p.m. in urban and suburban environments, where a typical speed limit is 65 mph (approximately 29 m/s). Fig. 4 presents a preliminary overview of the leading and following vehicle dynamics. The distributions of maximum speed, deceleration, and acceleration of vehicles are compared between HH and HA car-following cases.

Fig. 4 shows clear differences in movement between AV and HV leaders, as well as between HVs following AVs (HV followers in HA) and those following other HVs (HV followers in HH). The Lyft AVs tend to maintain a restrained maximum speed, predominantly at 12 m/s and 14 m/s. This restraint appears to have influenced the HVs following them in HA cases, resulting in a "compressed" distribution in maximum speed with a peak around 14 m/s. In terms of maximum acceleration, HVs in both HA and HH cases have similar distributions. However, compared with HV leaders and followers in HH cases, AV leaders and HV followers in HA cases experience larger maximum deceleration (around -2 m/s^2) more frequently and have fewer cases with a maximum deceleration near zero.

4.3. Inconsistent vehicle lengths

Using centroid-position data, accurate vehicle lengths are necessary for fine-grained analysis of spacing between vehicles. The data collected by AVs may be inconsistent in detecting the lengths of HVs directly behind the AVs and of HVs passing by the AVs. Fig. 5(a) presents the relationships between minimum gaps and detected vehicle lengths in the Lyft dataset (see Appendix A.2 for a counterpart in Waymo data). This figure shows that the HV lengths detected by AVs are independent of the proximity to AVs. However, the lengths of HA followers (HVs behind the AVs) deviate from the normally distributed lengths of HH followers and HH leaders (HVs passing by the AVs), and tend to be concentrated around 4.0 m and 5.0 m.

This inconsistency between HV lengths can influence the computed headways, particularly when the vehicles are at a slow speed or standing still. To roughly estimate this influence, we select stationary cases where both the leading and following vehicle speeds are smaller than 0.1 m/s, and plot the distributions of length sum $l_{follower} + l_{leader}$ as shown in Fig. 5(b). The average sum of leader and follower lengths for HH stationary cases is 8.79 m, while the average sum for HA stationary cases is 9.25 m. This difference can directly result in 0.23 m less average gap in HA cases than in HH cases, if assuming identical distributions of centroid-position distance. A specific magnitude of this influence on calculating distance headway, however, cannot be determined without ground-truth references. Therefore, we will compare time headway only in the rest of this study.
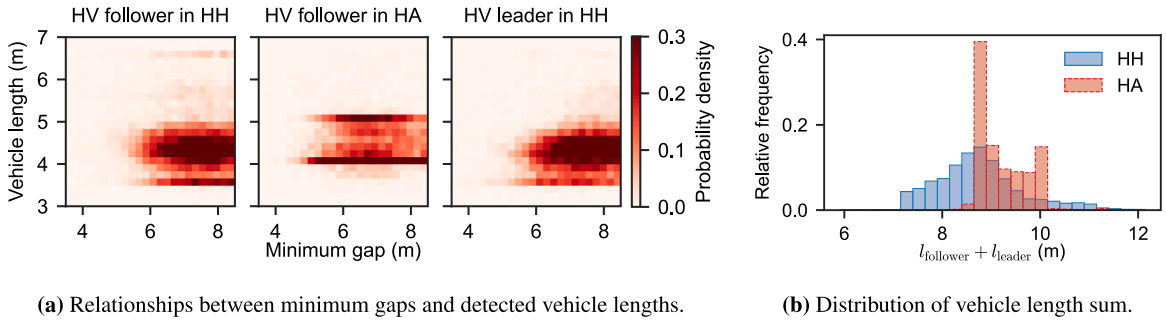
(a) Relationships between minimum gaps and detected vehicle lengths.

(b) Distribution of vehicle length sum.

Fig. 5. Inconsistency in length detection of human driving vehicles in HH and HA cases in Lyft data.
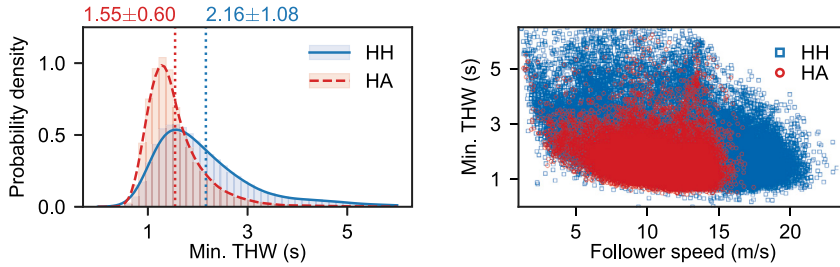

Fig. 6. Baseline comparison of time headway without isolating any factors.

4.4. Time headway reduction

An initial comparison of time headways between all HH cases and HA cases without isolating factors that may have effects, is displayed in Fig. 6. Here and throughout the next section, we use a uniform illustration to visually and quantitatively compare the time headways of HA and HH cases. This illustration is based on two considerations. First, time headway is infinite when the follower's speed is near zero. To dismiss those infinite values, we compare the distributions of minimum time headway (abbreviated as min. THW) of each car-following case, using histograms and their estimated probability densities. The mean values and standard deviations are also annotated in figures. Second, time headway depends on the current follower speed. We thus use a scatter plot showing the min. THW at various follower speeds, to offer a more comprehensive view.

Fig. 6, as a baseline, shows a tighter distribution of min. THW in HA cases than in HH cases. Observing the scatter plot of min. THW at different follower speeds, in most HA situations, the min. THW are within 4 s; while in many HH situations, the min THW are larger than 4 s and even exceed 6 s. Accordingly, the mean value and standard deviation of min. THW have a significant reduction in HA cases compared with HH cases. More specifically, the average min. THW is reduced by 0.61 s, and the standard deviation is 0.48 s smaller in HA cases than in HH cases. This reduction is consistent with the observations in existing literature. In the next section, we will detail the factors contributing to this reduction.

5. Results and discussion

This section presents and discusses the impacts of different factors on the reduction in time headway of human drivers following automated vehicles (AVs) compared to human driving vehicles (HVs). Sections 5.1, 5.2, and 5.3 are each about a factor among car-following states, leading driving variability, and AV driving characteristics. In Sections 5.2 and 5.3, we performed the Kolmogorov–Smirnov test in addition to the uniform illustration, to see whether the distributions under different settings are statistically different. The p-values and test results are annotated in figures based on a confidence level of 0.05. Finally, in Section 5.4, we make a summary of the findings for better reading.

5.1. Impact of car-following states

The composition of car-following states (regimes) is different in HH cases and HA cases. Using the method described in Section 3.1, we categorised the regimes at every time step in each car-following case of HA and HH. In Fig. 7, we present the time proportions of the regimes, including C: cruising at a desired speed, A: accelerating following a leader, D: decelerating following a leader, F: constant speed following, Fa: free accelerating less constrained by the leader, Fd: free decelerating less constrained by the leader, and S: staying stationary.
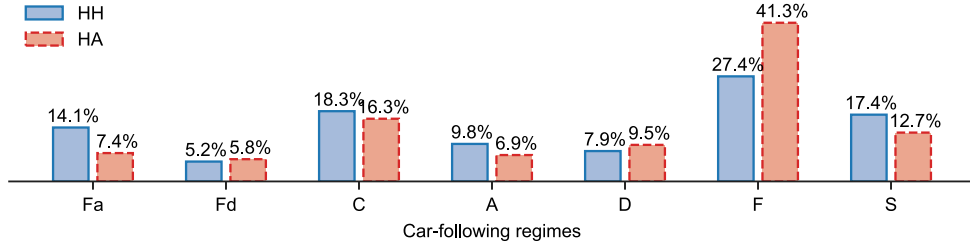
Fig. 7. Time proportion of different car-following regimes in HH cases and HA cases.

Table 3
Time proportion and average minimum time headway in different car-following regimes in HH and HA cases.

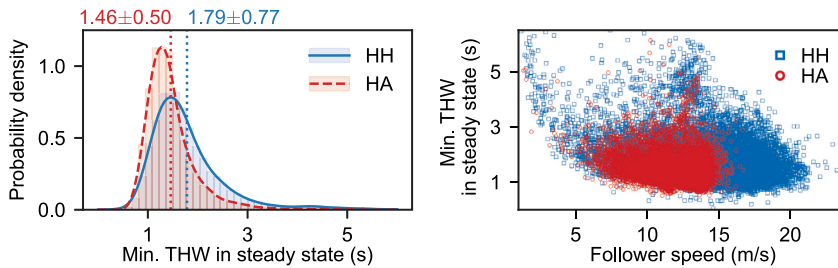| CF regime		Fa	C	Fd	D	A	F	S
HH	Time proportion (%)	8.99	11.01	7.42	23.22	11.09	38.27	0.00
	Average min. THW (s)	3.12	2.91	2.71	1.89	2.18	1.79	–
HA	Time proportion (%)	2.37	6.83	8.40	39.70	1.29	41.41	0.00
	Average min. THW (s)	2.06	2.10	2.06	1.40	1.77	1.46	–
THW Reduction (s)		1.06	0.81	0.65	0.49	0.41	0.33	–

Fig. 8. Time headway comparison with car-following states isolated.

Fig. 7 reveals distinct regime compositions between HH and HA cases. There is a similar proportion of time spent in cruising (C) but a significant difference in the constant speed following (F) regime. Given that time headway is smaller during constant-speed car-following than free-following, a reduction in time headway in HA cases is already reasonable. Interestingly, there is a higher occurrence of stationary moments (S) in HH cases compared to HA cases, which corresponds to an increased time proportion of free acceleration (Fa) or acceleration (A) after stopping. However, there is unexpectedly less time spent on deceleration (D) and free deceleration (Fd) in HH cases. This implies that the deceleration process in HH cases may be shorter than in HA cases.

According to the categorised car-following regimes, we can compare time headways in HH and HA cases under different car-following states. Table 3 compares the time proportion of each car-following regime as well as the corresponding average min. THW. These time proportions are accounted for the time steps when the minimum time headway is reached in a car-following case.

Most of the min. THW are reached in the regime F of constant-speed car-following, which accounts for 38.27% in HH cases and 41.41% in HA cases. Under the regime F, the average min. THW reduces by 0.33 s in HA cases compared to in HH cases. This constructs a fundamental part of the overall reduction in min. THW in HA cases. Generally in both HH and HA cases, the average values of min. THW are smaller in the car-following regimes of A, D, and F than in the free-following regimes of Fa, Fd, and C, where the leaders are less constrained by their followers. The reduction of min. THW is significantly larger in the regimes Fa (free acceleration) and C (cruising), accounting for 20.00% in HH cases but only 9.20% in HA cases. This is equivalent to averaging the min. THW with greater weights placed on the regimes that yield larger reductions, which exaggerates the extent of time headway reduction.

The reduction in time headway attracts attention majorly because it implies potential improvements in traffic efficiency. With this consideration, comparing time headways in HH and HA cases needs to be focused on steady-state car-following conditions. The leading and following vehicles do not interact with each other in free-following regimes (Fa, Fd, and C), i.e., the follower's time headways are not bounded by the leader and do not involve traffic. In the regimes of acceleration A and deceleration D, the followers are indeed affected by their leaders. However, followers in such situations need to make a trade-off between avoiding collision and chasing up, which makes the resulted time headways unrepresentative. Therefore, in Fig. 8 and the subsequent comparisons, we consider min. THW in the regime F only. The focus on steady-state time headways relates more directly to potential traffic benefits.

In Fig. 8, the average min. THW is 1.46 s in HA cases and 1.79 s in HH cases, and the distribution of min. THW remains tighter in HA cases than in HH cases. The differences become significantly less when compared with that in Fig. 6. More specifically, the
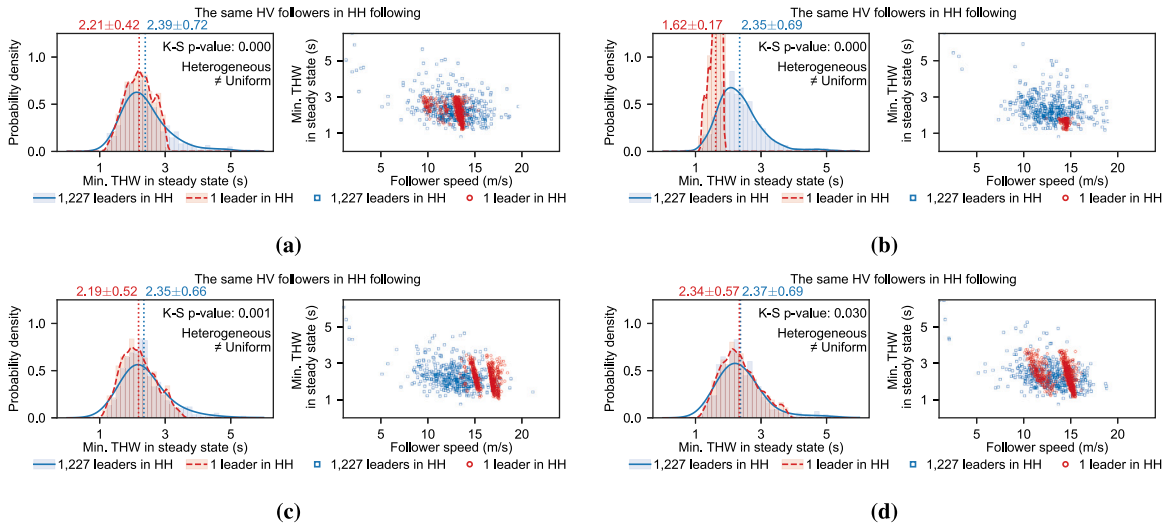
Fig. 9. Time headway comparisons with driving variability isolated. Four different single leading vehicles are simulated as the uniform leader driving in subfigures (a), (b), (c) and (d). The simulations use Intelligent Driver Models.

reduction of average min. THW decreases from 0.61 s to 0.33 s after excluding non-steady regimes. The standard deviations in both the HA and HH cases are also considerably smaller. These are also reflected in the scatter plot, where the min. THW in both HA and HH cases are more concentrated within 3 s.

5.2. Impact of driving variability

Analysing AV-involved data can face a problem that does not exist in traditional HV-only datasets: the driving variability of leading vehicles is highly unbalanced. In the Lyft dataset, there are 20 Lyft leading AVs in HA cases, while 42,982 different leading HVs in HH cases. The 20 AV leaders share the same Lyft's autonomous driving algorithms, which implies a substantially lower variability of leader driving behaviour in HA cases than in HH cases. This imbalance may significantly influence the statistical comparison of time headways between HH and HA cases. Following the methods in Section 3.2.1, we calibrated two sets of Intelligent Driver Models (IDMs) for HH cases and HA cases. For details about the calibration results, see Appendix A.3.

We obtained 1228 eligible HH cases and calibrated their corresponding IDMs, based on which we then conducted controlled simulation experiments. Fig. 9 shows the comparisons of minimum time headways in the simulation experiments, where the same 1227 HV followers follow a single HV leader or 1227 heterogeneous HV leaders, respectively. For a more robust assessment of the leader variability effect, 4 different single leaders are involved in parallel simulations.

Fig. 9 shows that following a single leader can result in a significantly smaller mean value (0.275 s on average) and standard deviation (0.27 s on average) of min. THW. This is also clearly seen in the scatter plots, where the minimum time headways concentrate at certain follower speeds when following a single leader but disperse over various follower speeds when following many different leaders. In Appendix A.4, the counterpart simulations using Gipps' model show similar results, with average reductions in mean value by 0.31 s and in standard deviation by 0.21 s. These comparisons suggest that uniform AV driving plays an important role in the reduced time headways in HA cases, against heterogeneous HV driving in HH cases. Additionally, as revealed by comparing across the 4 simulations of following different single leaders, the leader's driving characteristics also contribute remarkably to time headway distributions. The next subsection will investigate this further.

5.3. Impact of AV driving characteristics

AVs drive differently from HVs. This difference in driving dynamics may create different car-following contexts for human drivers following AVs versus HVs. To distinguish AV driving and HV driving characteristics, we trained a neural network classifier as described in Section 3.3. The classifier can correctly classify 95.95% of AV driving segments and 92.66% of HV driving segments in the training data, reaching an overall accuracy of 94.24%; while on the validation set, it can correctly classify 94.12% and 90.59% of AV and HV driving segments, respectively. For more details about the training evolution and performance evaluation, see Appendix A.5.

The classifier captures the difference in stability between AV driving and HV driving, i.e., more stable driving is more probable to be classified as of an AV. As mentioned in Section 3.3, constantly stationary trajectory segments were excluded during model training and validation. Here we create multiple stationary zero-speed trajectory segments, as out-of-distribution inputs, to test the classifier. Each of the created segments consists of 148×2 random numbers from a zero-mean normal distribution, where the
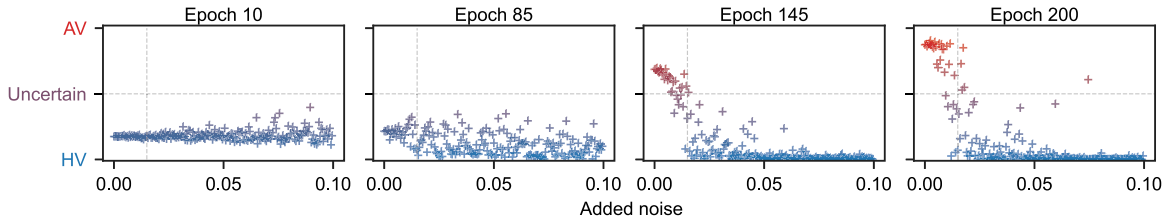
Fig. 10. Classifications of stationary trajectory segments with randomly added noises.

(a) Comparison between HV-like and AV-like cases.

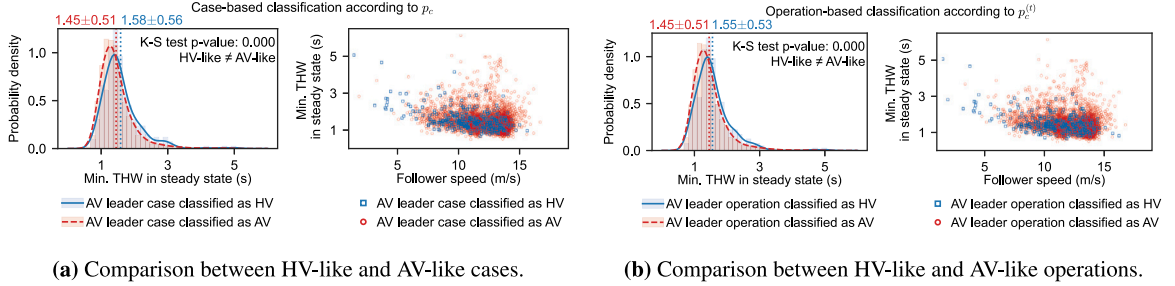**(b)** Comparison between HV-like and AV-like operations.

Fig. 11. Comparison of time headway with driving characteristics isolated. HV-like refers to an AV leader case/operation being classified as HV; AV-like refers to an AV leader case/operation being classified as AV.

standard deviation increases from 0 to 0.1 as added noise. Fig. 10 shows the classification of these stationary segments in different stages of model training. With the training progresses, the classifier gradually learns to distinguish AV driving and HV driving by stability. As shown in Epochs 145 and 200, When the added noise is smaller than around 0.015, the stationary trajectory tends to be classified as AV driving; however, when the added noise is larger, the stationary trajectory tends to be classified as HV driving.

We postulated that the unique driving characteristics of Lyft AVs impact the headway reduction in HA cases if human drivers have longer headways when following AVs resembling human driving. By applying the trained classifier to the 13,814 HA cases[2] in the validation set, we have 1104 cases where the AV leaders are "incorrectly" classified as driving more like an HV ($p_c < 0.5$, abbreviated as HV-like); in the other 12,710 cases, the AV leaders are classified as driving more like an AV ($p_c > 0.5$, abbreviated as AV-like). These HV-like and AV-like driving operations of AVs allow us to isolate the factor of driving characteristics, control for the factor of driving variability, and effectively observe the impact. The distributions of min. THW in these cases are displayed in Fig. 11. In Fig. 11(a), the classification between HV-like and AV-like time headways is case-based according to p_c; while in Fig. 11(b), the classification is operation-based according to $p_c^{(t)}$.

Both Figs. 11(a) and 11(b) have HVs following AVs. Despite the leading vehicle driving are both performed by AVs, the distributions and scatter plots clearly show that the min. THW is generally larger for HV-like driving than AV-like driving. More specifically, the average min. THW in HV-like driving cases is 0.13 s larger than in AV-like driving cases; the average min. THW under HV-like driving operations is 0.10 s larger than AV-like driving operations. This suggests a considerable impact of driving characteristics on the reduced headways of human drivers following AVs. However, except for stability, it remains to be investigated what characteristics lead to the reduction.

5.4. Summary of main findings

This section explored potential explanations for the reduction in headways of human drivers following AVs than following HVs. Due to the inconsistent detection of vehicle lengths between HVs passing by and directly following AVs, only time headway was considered in our examinations. For the examined 3 factors alternative to behavioural changes of following vehicle drivers, we utilised a variety of methods to isolate each of them and assess their impacts, and now summarise the main findings.

- **Systematic differences in car-following states during data collection**. The data collected of HV-following-AV and HV-following-HV have different percentages of car-following states such as cruising, decelerating, steady-state following, staying stationary, etc. Time headways are generally larger in non-steady car-following states. Therefore, the smaller proportion of non-steady states in HV-following-AV data than in HV-following-HV data directly results in a shorter average time headway. To better relate with potential traffic benefits that AVs can bring, we focus on time headways under steady-state car-following. In doing so, the reduction in average time headway of HVs following AVs shrinks to 0.33 s from 0.61 s that is calculated without isolating any factors.

---

[2] Among the 29,449 HA cases, 1822 cases are excluded because of a stationary process exceeding 14.8 s. Of the remaining 27,627 cases, half are assigned to the training set and the other half to the validation set.

- **Systematic differences in driving variability between leading AVs and HVs**. The leading Lyft AVs in HV-following-AV cases share the same driving algorithms, while the leading HVs in HV-following-HV cases have heterogeneous driving styles. The homogeneity of leading vehicles' driving can be transmitted to their following vehicles' driving, and thus decreases the variance of time headway distribution and shortens the average. In our experiments, letting various HVs follow the same HV resulted in an average reduction in steady-state time headway by 0.275 s (simulated with the Intelligent Driver Model) and 0.31 s (simulated with Gipps' model) compared to following different HVs with heterogeneous driving styles.

- **Systematic differences in driving characteristics of leading AVs versus HVs**. The specific driving characteristics of AVs, such as stability, also have a remarkable impact. When human drivers follow AVs that drive like HVs, the average time headway is approximately 0.10 s larger than following AVs that drive more stably like AVs. Interestingly, Soni et al. (2022) observed no reduction in headway when human drivers follow a "Wizard of Oz" AV (i.e., the leading vehicle was operated in reality by a human, but the participants were informed that they were following an AV) compared with following an HV. Therefore, human drivers may not consciously maintain a shorter distance when following AVs, but they can be unconsciously influenced if the leading AVs drive differently than HVs.

Other than behavioural changes of followers, these findings provide quantitative assessments of three alternative explanations for the reduced time headways behind AVs. However, these assessment results cannot be simply added together. The effects of these factors interplay with each other in practice, and disentangling the interplay necessitates further investigation. In addition, it is important to note that these findings do not exclude behavioural changes due to factors such as the following vehicle drivers' perceived reliability of AVs or desire to interact with AVs. Behavioural factors remain intangible in the absence of direct evidence on driver perception and preference, and require future research.

6. Conclusion and outlook

This study advances a more comprehensive understanding of the interactions between human driving vehicles and automated vehicles compared to the interactions between human drivers, and the contribution is twofold. First, we provide an approach to examining the impacts of integrating automated vehicles on average time headway with empirical data, particularly in the mixed traffic environment. We point out inherent observation biases when using data collected by automated vehicles to compare human drivers' interactions with automated vehicles and the interactions between human drivers. The biases are induced by factors such as various car-following states during data collection, uniformity of autonomous driving algorithm against heterogeneity of human driving, and the distinct characteristics of autonomous driving. Employing different methods, we isolated these factors and examined their impacts. Second, through careful examination, this study offers more in-depth insights explaining the consistently observed shorter headways when human drivers follow automated vehicles compared to following human driving vehicles. Beyond the speculation of human drivers' behavioural changes, the observation biases rooted in such a comparison play remarkable (probably primary) roles. This study thus serves as a reminder for researchers to be cautious when drawing behavioural insights from "non-behavioural" data, and to be sceptical about the efficiency benefits of integrating automated vehicles. Furthermore, we suggest that careful experimental design is needed to control the comparison conditions for investigating behavioural changes of human drivers in the presence of automated vehicles.

From a lens of human drivers' adaption to automated vehicles, this study proceeds towards more effective integration of automated vehicles into human traffic for enhancing traffic efficiency. In pursuit of this end, more research is needed in the future. Except for time headway, the potential reduction in the minimum gap or distance headway when human drivers follow AVs necessitates more reliable measurement and further research on the decelerating process, which also includes safety concerns. This study is based on the data collected in an urban environment, where the traffic is not continuous and is disrupted by red lights and interactions with other road users such as pedestrians. These disruptions may exacerbate the reduction in time headway, and it is unclear whether such reduction is smaller on highways. Our findings suggest that homogeneous and stable driving can lead to a reduction in steady-state time headway, regardless of human-driven or machine-driven. However, traffic performance is not only about shorter time headway, but also relates to string stability and demand control. Figuring out all these factors' influences will help to integrate automated vehicles into existing transportation systems. This then, as expected, will reduce traffic congestion and energy consumption, and ultimately promote a more efficient and sustainable traffic environment.

CRediT authorship contribution statement

Data availability

We open-source our code for repeating experiments and reuse at https://github.com/Yiru-Jiao/Explaining-headway-reduction-of-HVs-following-AVs.

Declaration of Generative AI and AI-assisted technologies in the writing process

During the preparation of this work the authors used ChatGPT in order to seek suggestions for readability improvement. No sentence was entirely generated by ChatGPT. After using this tool/service, the authors reviewed and edited the content as needed and take full responsibility for the content of the publication.

Acknowledgements

Appendix

A.1. Algorithm to identify car-following regimes

Here we present more details about the algorithm to identify car-following (CF) regimes. Our code for implementing this algorithm is also open-sourced. The algorithm takes 7 inputs as shown in Algorithm A1. Using the same notation as in Eq. (1), the positions and speeds along time t of a leader are respectively x_{leader} and v_{leader}. In parallel, the follower's positions and speeds are x_{follower} and v_{follower}. In addition, μ_{all} and σ_{all} are the mean value and standard deviation of time gaps calibrated from all cases of HA or HH using Newell's car-following model. Algorithms A2 and A3 are called in Algorithm A1 as preliminaries.

Algorithm A1: Car-following regime determination

Input: $t, x_{\mathrm{leader}}, x_{\mathrm{follower}}, v_{\mathrm{leader}}, v_{\mathrm{follower}}, \mu_{\mathrm{all}}, \sigma_{\mathrm{all}}$
Output: Car-following regimes r corresponding each time step in t

1   $s_v \leftarrow \mathrm{SpeedSegmentation}(t, v_{\mathrm{follower}})$
2   $f \leftarrow \mathrm{DistinguishCForFF}(t, x_{\mathrm{leader}}, x_{\mathrm{follower}}, v_{\mathrm{leader}}, v_{\mathrm{follower}}, \mu_{\mathrm{all}}, \sigma_{\mathrm{all}})$
3   **foreach** s **in** s_v **do**
4      $t_s, v_s, f_s \leftarrow$ segments of $t, v_{\mathrm{follower}}, f$ corresponding to s
5      $\hat{a} \leftarrow \Delta v_s / \Delta t_s$ // Calculate the change rate of follower speed within the segment, m/s^2
6      $\bar{v} \leftarrow$ average of v_s
7   **if** there are more free-following than car-following in f_s **then**
8   **if** $|\hat{a}| \leq 0.5$ **then**
9   **if** $\bar{v} < 0.1$ **then**
10   regime $\leftarrow$ S
11   **else**
12   regime $\leftarrow$ C
13   **end**
14   **else if** $\hat{a} > 0.5$ **then**
15   regime $\leftarrow$ Fa
16   **else**
17   regime $\leftarrow$ Fd
18   **end**
19   **else**
20   **if** $|\hat{a}| \leq 0.5$ **then**
21   **if** $\bar{v} < 0.1$ **then**
22   regime $\leftarrow$ S
23   **else**
24   regime $\leftarrow$ F
25   **end**
26   **else if** $\hat{a} > 0.5$ **then**
27   regime $\leftarrow$ A
28   **else**
29   regime $\leftarrow$ D
30   **end**
31   **end**
32      $r_s \leftarrow$ regime   // r_s has the same shape as t_s
33   **end**
34   Combine r_s for each s in s_v into r
35   **return** r

Algorithm A2: Speed profile segmentation

---

1 **Function** SpeedSegmentation(t, v):
　　Input: time series t, speed series v
　　Output: divided segments of speed s_v
2 　$s_v \leftarrow v$ 　　　　　　　　　　　　　　　　// Each speed point starts as a segment
3 　$n \leftarrow \text{len}(t)$ 　　　　　　　　　　　　　　　　　// Set number of segments
4 　$n_{\max} = (\max(t) - \min(t))/0.5$ 　　　　// Set max. number of segments based on time duration
5 　**while** $n > n_{\max}$ **do**
6 　　**foreach** s in s_v **do**
7 　　　Calculate the cost of merging s and its adjacent segments
8 　　**end**
9 　　Merge adjacent segments with the minimum cost
10 　　Merge any consecutive segments if they have similar slopes
11 　　Update s_v and calculate n
12 　**end**
13 　**return** s_v

Algorithm A3: Car-following and Free-following distinguishment

---

1 **Function** DistinguishCForFF($t, x_{leader}, x_{follower}, v_{leader}, v_{follower}, \mu_{all}, \sigma_{all}$):
　　Input: time series t, positions $x_{leader}, x_{follower}$, speeds $v_{leader}, v_{follower}$, thresholds μ_{all}, σ_{all}
　　Output: series of following regimes f
2 　$W \leftarrow$ a warping path by applying Dynamic Time Warping (DTW) to x_{leader} and $x_{follower}$
3 　$\tau \leftarrow$ time differences between the aligned elements in W
4 　**if** half of τ are less than 0.1 second **then**
5 　　$W \leftarrow$ a warping path by applying Dynamic Time Warping (DTW) to v_{leader} and $v_{follower}$
6 　　$\tau \leftarrow$ time differences between the aligned elements in W
7 　**end**
8 　Replace $\tau < 0.1$ in τ with its neighbouring τ that are larger than 0.1 second
9 　Compress τ to match the length of t
10 　$\mu_\tau, \sigma_\tau \leftarrow$ mean value and standard deviation of τ
11 　**if** $\mu_\tau > \mu_{all}$ **or** $\sigma_\tau > \sigma_{all}$ **then**
12 　　$\tau_{\text{threshold}} \leftarrow \mu_\tau$
13 　**else**
14 　　$\tau_{\text{threshold}} \leftarrow \mu_\tau + 2\sigma_\tau$
15 　**end**
16 　$f \leftarrow$ car-following if the corresponding $\tau < \tau_{\text{threshold}}$, otherwise free-following
17 　**return** f

---

A.2. Vehicle length detection bias in Waymo data

Fig. A1(a) shows the relationships between minimum gaps and detected vehicle lengths in the Waymo dataset. Due to relatively less data than the Lyft data, here we directly plot scatters rather than histograms. This figure conveys the same message as Fig. 5(a): the lengths of HVs following the AV (in HA cases) are generally larger than the lengths of HV leaders and followers in HH cases (HVs passing by the AV). This inconsistency further affects the computed headways. The histograms in Fig. A1(b) show the rough impacts estimated in the same way as in Fig. 5. As a result, the average sum of leader and follower lengths for HH stationary cases is 9.64 m, while in HA stationary cases this value is 10.32 m. In Waymo data, this bias in vehicle length detection can lead to a reduction of 0.34 m in the minimum gap in HA cases than in HH cases.

A.3. IDM calibration results

We used evolutionary algorithm to solve the optimisation in Eq. (5). According to Zhang and Sun (2024), v_0 and δ would converge to their priors if calibrated simultaneously. In order to keep the calibration stable, we fix $\delta = 4$ following typical settings. The other parameters are then optimised within corresponding bounds. v_0 is set to be between 12 and 29 m/s. We also dynamically set other bounds based on the meaning of the parameters. This includes $\min(\text{DHW}) - 0.2 \leq s_0 \leq 20$ m, $\max(0.5, \min(\text{THW}) - 0.2) \leq T \leq 10$ s, $0.3 \leq \alpha \leq \max(a_{\text{follower}}) + 1.5$ m/s^2, and $\min(a_{\text{follower}}) - 0.2 \leq \beta \leq 6$ m/s^2, where DHW, THW, and a_{follower} are distance headway, time headway, and acceleration series in a car-following case.

As presented in Table A.1, the calibrations with human-following-human (HH) cases have mean absolute errors of 0.38 ± 0.14 m/s^2 in acceleration and of 0.46 ± 0.20 m/s in speed; the calibrations with human-following-AV (HA) cases has slightly smaller mean absolute errors of 0.31 ± 0.11 m/s^2 in acceleration and of 0.44 ± 0.43 m/s in speed.
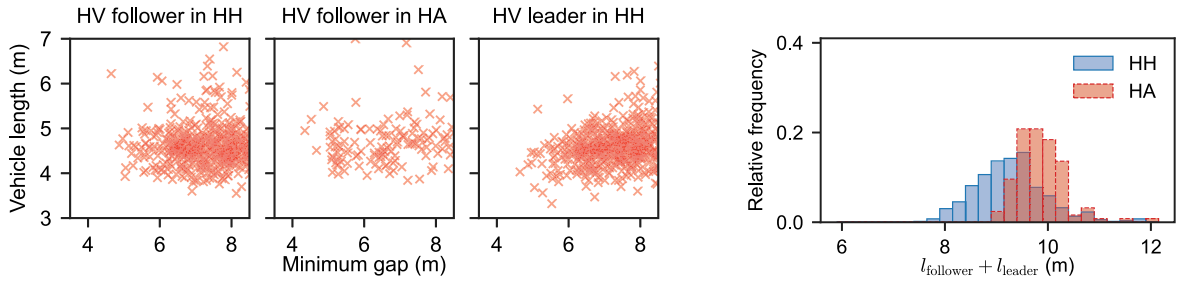
(a) Relationships between minimum gaps and detected vehicle lengths.

(b) Distribution of vehicle length sum.

Fig. A1. Inconsistency in length detection of human driving vehicles in HH and HA cases in Waymo data.

Table A.1
Accuracy evaluation of calibrating Intelligent Driver Models for HH cases and HA cases.

		Acceleration (m/s^2)	Speed (m/s)	Position (m)
HH (1,228)	MAE	0.38 ± 0.14	0.46 ± 0.20	3.49 ± 1.74
Mean±Std.	RMSE	0.56 ± 0.26	0.61 ± 0.25	4.45 ± 2.16
HA (1,323)	MAE	0.31 ± 0.11	0.44 ± 0.43	3.32 ± 4.98
Mean±Std.	RMSE	0.45 ± 0.22	0.56 ± 0.45	4.00 ± 5.58

MAE: mean absolute error; RMSE: root mean squared error.

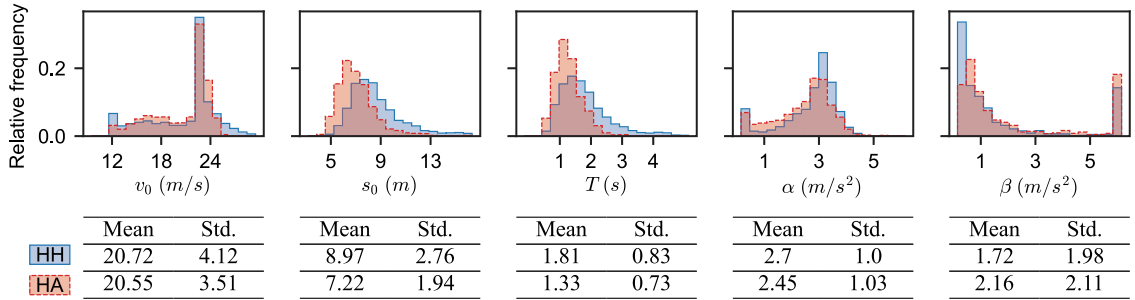|	Mean	Std.	Mean	Std.	Mean	Std.	Mean	Std.	Mean	Std.
HH	20.72	4.12	8.97	2.76	1.81	0.83	2.7	1.0	1.72	1.98
HA	20.55	3.51	7.22	1.94	1.33	0.73	2.45	1.03	2.16	2.11

Fig. A2. Comparison of the calibrated Intelligent Driver Model parameters for HH cases and HA cases.

Fig. A2 then compares the calibrated IDM parameter distributions of the HH cases and the HA cases. In addition to the histograms, the averages and standard deviations of each parameter are listed in the tables beneath the plots. On average, HH cases have larger desired speeds v_0, longer minimum distance headway s_0, and longer desired time headway T. These tendencies make no surprise as they are bound to the corresponding empirical estimations in our calibration. Meanwhile, evidently smaller variances of the parameters v_0, s_0, and T are seen in HA cases. This indicates a lower driving variability of HV followers in HA cases. Interestingly, the maximum acceleration α in many HA cases is smaller than in HH cases, while the comfortable deceleration β is significantly larger than in HH cases. This is aligned with Fig. 4 in Section 4.1, suggesting that there are more brakings and potentially less safe driving situations when HVs follow AVs.

A.4. Simulation experiments based on Gipps' model

To offer corroborating evidence for the impact of leading vehicles' driving variability, we conducted the simulation experiments in Section 3.2.2 using Gipps' car-following model in addition to the Intelligent Driver Model (IDM). Except for the car-following model, we used the same experiment settings as when using IDM, including the calibration method and objective function, simulation experiment design, and results evaluation.

As defined in Eq. (A.1), Gipps' model assumes that a driver adapts the speed after a time delay (τ) to either smoothly reach the desired speed or to safely proceed behind the leader (Ciuffo et al., 2012; Vieira da Rocha et al., 2015). Here v^{acc} is the speed for the first purpose, and v^{dec} is for the second purpose. Different from IDM which maps the stimuli to acceleration, Gipps' model produces speed profiles. Correspondingly, we update the following vehicle's positions as shown in Eq. (A.2).

$$v(t + \tau) = \min\{v^{acc}(t + \tau), v^{dec}(t + \tau)\} \tag{A.1}$$

$$\hat{x}(t + \tau) = x(t) + \frac{v(t) + v(t + \tau)}{2}\tau \tag{A.2}$$

Table A.2
Accuracy evaluation of calibrating Gipps' models for HH cases and HA cases.

		Speed (m/s)	Position (m)
HH (1,228)	MAE	0.63 ± 0.29	2.94 ± 1.58
Mean±Std.	RMSE	0.83 ± 0.38	3.74 ± 2.05
HA (1,323)	MAE	0.45 ± 0.56	2.81 ± 5.70
Mean±Std.	RMSE	0.59 ± 0.64	3.43 ± 6.29

MAE: mean absolute error; RMSE: root mean squared error.

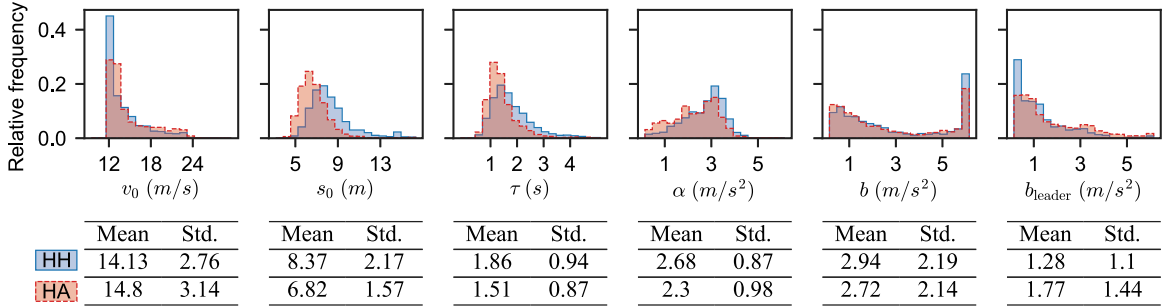|	v_0 (m/s)		s_0 (m)		τ (s)		α (m/s²)		b (m/s²)		b_{leader} (m/s²)	
	Mean	Std.	Mean	Std.	Mean	Std.	Mean	Std.	Mean	Std.	Mean	Std.
HH	14.13	2.76	8.37	2.17	1.86	0.94	2.68	0.87	2.94	2.19	1.28	1.1
HA	14.8	3.14	6.82	1.57	1.51	0.87	2.3	0.98	2.72	2.14	1.77	1.44

Fig. A3. Comparison of the calibrated Gipps' model parameters for HH cases and HA cases.

Eqs. (A.3) show more details of the speed adjustment in Gipps' model. For comparison convenience, we use the same notation as in IDM to explain the parameters. The movement states of a vehicle (follower) and its preceding vehicle (leader) during car-following are described with three variables: $v(t)$ is the follower speed at the time t, $s(t)$ is the distance between the leader and the follower, and $\Delta v(t)$ is their relative speed.

$$\begin{cases} v^{acc}(t+\tau) = v(t) + 2.5\alpha\tau\left(1 - \frac{v(t)}{v_0}\right)\sqrt{0.025 + \frac{v(t)}{v_0}} \\ v^{dec}(t+\tau) = -\tau b + \sqrt{\tau^2 b^2 + b\left[2\left(s(t) - s_0\right) - \tau v(t) + \frac{(v(t) - \Delta v(t))^2}{b_{leader}}\right]} \end{cases} \quad (A.3)$$

There are 6 parameters to be calibrated in the Gipps' model. Each of the parameters corresponds to a practical meaning: v_0 is the desired speed of the follower, s_0 is the minimum distance headway, τ is the delay integrating both time headway and reaction time, α and b are respectively the maximum acceleration and deceleration of the follower, and b_{leader} is the maximum deceleration of the leader expected by the follower. In the use of this model, to make sure $v^{dec} \geq 0$, we take 0 for v^{dec} if $2\left(s(t) - s_0\right) - \tau v(t) + (v(t) - \Delta v(t))^2 / b_{leader} < 0$.

The accuracy evaluation of Gipps' model calibration is presented in Table A.2, where the mean absolute error of speed is 0.63 ± 0.29 m/s with HH cases and 0.45 ± 0.56 m/s with HA cases. This is slightly larger than the calibration error of using IDM. In Fig. A3, the distributions of parameters calibrated with HH and HA cases are shown in the same format as in Fig. A2. Compared with the calibrated parameters of IDM in Fig. A2, s_0, τ and α have similar distributions, while v_0 is more concentrated to smaller speeds when using Gipps' model.

Fig. A4 shows the comparisons of minimum time headways (min. THW) in the controlled simulation experiments using Gipps' model. Although the scatters of min. THW along follower speed are differently distributed from those in the simulations using IDM in Fig. 9, the conclusion is the same. In these simulation experiments applying Gipps' model, the min. THW in steady states when following a single HV leader has an average reduction in mean value by 0.31 s and in standard deviation by 0.21 s, compared to following heterogeneous HV leaders.

A.5. Classifier evaluation

We trained the model for 200 epochs (i.e. iterations) and recorded the training performance per every 5 epochs. The evolution of average loss, accuracy and F1 score (defined as the harmonic mean of precision and recall) is shown in Fig. A5. The model was well-trained as indicated by the decreasing average loss. The overfitting starts after around 150 epochs, as indicated by the increasing training accuracy while the validation accuracy remains constant and test accuracy becomes a bit lower. Therefore, we select the one after 145 epochs of training as the model to use.

Applying the trained classifier to the AV leaders in the validation set gives 1104 AV leaders driving like HVs. Figs. A6 display the captured differences in driving dynamics of AV leaders between HV-like and AV-like. For a more comparable analysis, the maximum speed is counted for each car-following case if in the regime C (cruising) or F (constant speed car-following), the maximum acceleration is counted if in the regime A (acceleration) or Fa (free acceleration), and the maximum deceleration is counted if in the regime D (deceleration) or Fd (free deceleration).
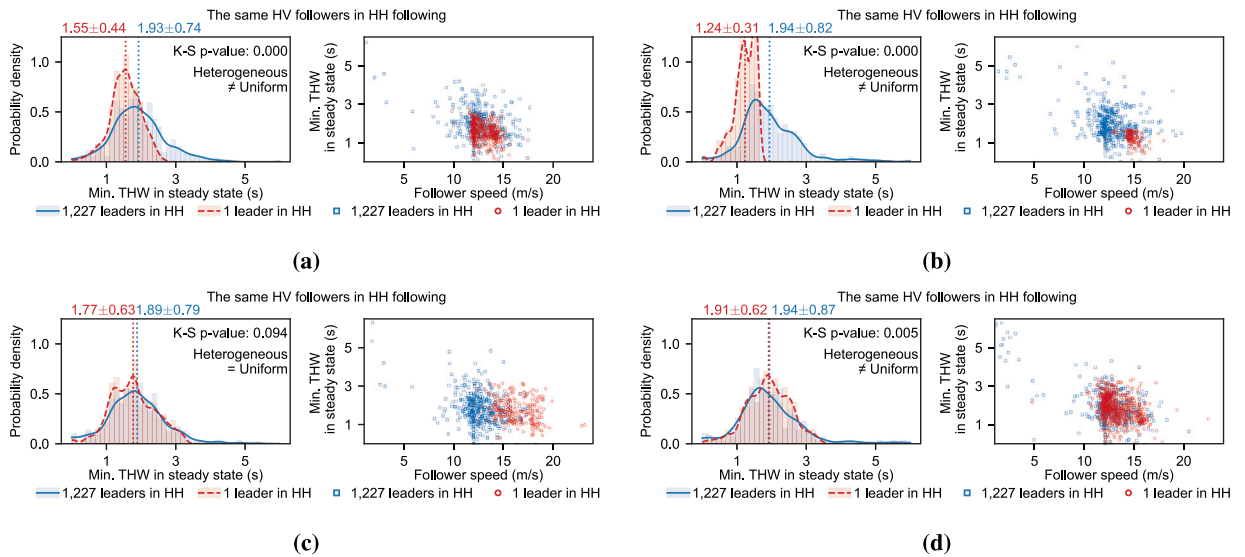
(a)

(b)

(c)

(d)

Fig. A4. Time headway comparisons with driving variability isolated. Four different single leading vehicles are simulated as the uniform leader driving in sub-figures (a), (b), (c), and (d). The simulations use Gipps' car-following model.
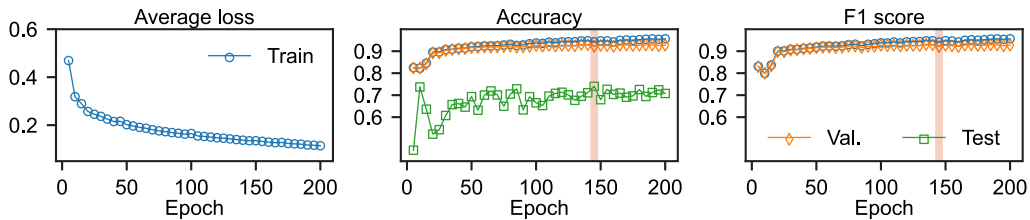

Fig. A5. Evaluation and selection of the classifier neural networks.
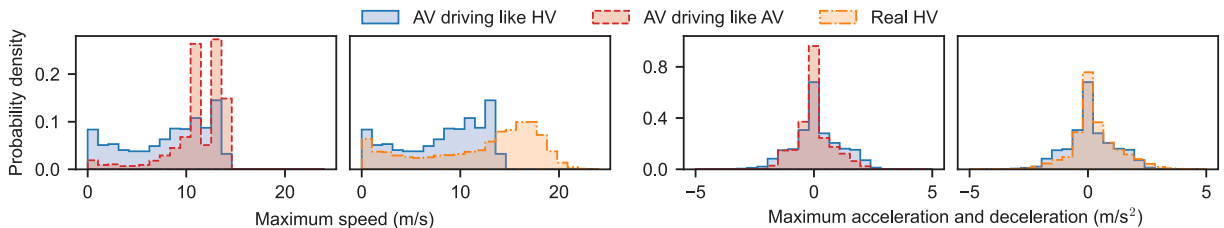

Fig. A6. Comparison of maximum speeds, accelerations, and decelerations between AV-like, HV-like, and real HV driving.

Due to the speed restriction on Lyft AVs, The classified HV-like driving does not exactly match the characteristics of real HV driving in Fig. A6. Nevertheless, the classifier distinguishes two evidently different patterns in terms of speed and ac/deceleration. More specifically, AV-like driving has more discrete maximum speeds, smaller maximum acceleration, but larger maximum deceleration, than HV-like driving. These characteristics are aligned with the comparison between real AV driving and HV driving in Fig. 4.

References

Aittoniemi, E., 2022. Evidence on impacts of automated vehicles on traffic flow efficiency and emissions: Systematic review. IET Intell. Transp. Syst. 16 (10), 1306–1327. http://dx.doi.org/10.1049/itr2.12219.

Albeaik, S., Bayen, A., Chiri, M.T., Gong, X., Hayat, A., Kardous, N., Keimer, A., McQuade, S.T., Piccoli, B., You, Y., 2022. Limitations and improvements of the intelligent driver model (IDM). SIAM J. Appl. Dyn. Syst. 21 (3), 1862–1892. http://dx.doi.org/10.1137/21m1406477.

Aria, E., Olstam, J., Schwietering, C., 2016. Investigation of automated vehicle effects on driver's behavior and traffic performance. Transp. Res. Procedia 15, 761–770. http://dx.doi.org/10.1016/j.trpro.2016.06.063.

Barmpounakis, E., Geroliminis, N., 2020. On the new era of urban traffic monitoring with massive drone data: The pNEUMA large-scale field experiment. Transp. Res. C 111, 50–71. http://dx.doi.org/10.1016/j.trc.2019.11.023.

Bian, Y., Zheng, Y., Ren, W., Li, S.E., Wang, J., Li, K., 2019. Reducing time headway for platooning of connected vehicles via V2V communication. Transp. Res. C 102, 87–105. http://dx.doi.org/10.1016/j.trc.2019.03.002.

Caesar, H., Bankiti, V., Lang, A.H., Vora, S., Liong, V.E., Xu, Q., Krishnan, A., Pan, Y., Baldan, G., Beijbom, O., 2020. nuScenes: A multimodal dataset for autonomous driving. In: Proceedings of the IEEE/CVF Conference on Computer Vision and Pattern Recognition. CVPR.

Calvert, S.C., Schakel, W.J., van Lint, J.W.C., 2017. Will automated vehicles negatively impact traffic flow? J. Adv. Transp. 2017, 1–17. http://dx.doi.org/10.1155/2017/3082781.

Carlsen, A.N., Maslovat, D., Kaga, K., 2020. An unperceived acoustic stimulus decreases reaction time to visual information in a patient with cortical deafness. Sci. Rep. 10 (1), http://dx.doi.org/10.1038/s41598-020-62450-9.

Chang, M.-F., Lambert, J., Sangkloy, P., Singh, J., Bak, S., Hartnett, A., Wang, D., Carr, P., Lucey, S., Ramanan, D., Hays, J., 2019. Argoverse: 3D tracking and forecasting with rich maps. In: Proceedings of the IEEE/CVF Conference on Computer Vision and Pattern Recognition. CVPR, Carlifornia, United States.

Ciuffo, B., Punzo, V., Montanino, M., 2012. Thirty years of gipps' car-following model: Applications, developments, and new features. Transp. Res. Rec.: J. Transp. Res. Board 2315 (1), 89–99. http://dx.doi.org/10.3141/2315-10.

Coifman, B., Wu, M., Redmill, K., Thornton, D.A., 2016. Collecting ambient vehicle trajectories from an instrumented probe vehicle. Transp. Res. C 72, 254–271. http://dx.doi.org/10.1016/j.trc.2016.09.001.

Di, X., Shi, R., 2021. A survey on autonomous vehicle control in the era of mixed-autonomy: From physics-based to AI-guided driving policy learning. Transp. Res. C 125, 103008. http://dx.doi.org/10.1016/j.trc.2021.103008.

Duarte, F., Ratti, C., 2018. The impact of autonomous vehicles on cities: A review. J. Urban Technol. 25 (4), 3–18. http://dx.doi.org/10.1080/10630732.2018.1493883.

Gipps, P., 1981. A behavioural car-following model for computer simulation. Transp. Res. B 15 (2), 105–111. http://dx.doi.org/10.1016/0191-2615(81)90037-0.

Hamdar, S., 2012. Driver behavior modeling. In: Eskandarian, A. (Ed.), Handbook of Intelligent Vehicles. Springer, London, pp. 537–558. http://dx.doi.org/10.1007/978-0-85729-085-4_20.

Hochreiter, S., Schmidhuber, J., 1997. Long short-term memory. Neural Comput. 9 (8), 1735–1780. http://dx.doi.org/10.1162/neco.1997.9.8.1735.

Houston, J., Zuidhof, G., Bergamini, L., Ye, Y., Chen, L., Jain, A., Omari, S., Iglovikov, V., Ondruska, P., 2021. One thousand and one hours: Self-driving motion prediction dataset. In: Kober, J., Ramos, F., Tomlin, C. (Eds.), In: Proceedings of the 2020 Conference on Robot Learning, vol. 155, pp. 409–418.

Hu, X., Zheng, Z., Chen, D., Sun, J., 2023. Autonomous vehicle's impact on traffic: Empirical evidence from Waymo open dataset and implications from modelling. IEEE Trans. Intell. Transp. Syst. 1–14. http://dx.doi.org/10.1109/tits.2023.3258145.

Hu, X., Zheng, Z., Chen, D., Zhang, X., Sun, J., 2022. Processing, assessing, and enhancing the waymo autonomous vehicle open dataset for driving behavior research. Transp. Res. C 134, 103490. http://dx.doi.org/10.1016/j.trc.2021.103490.

Hulse, L.M., Xie, H., Galea, E.R., 2018. Perceptions of autonomous vehicles: Relationships with road users, risk, gender and age. Saf. Sci. 102, 1–13. http://dx.doi.org/10.1016/j.ssci.2017.10.001.

Krajewski, R., Bock, J., Kloeker, L., Eckstein, L., 2018. The highd dataset: A drone dataset of naturalistic vehicle trajectories on german highways for validation of highly automated driving systems. In: IEEE 21st International Conference on Intelligent Transportation Systems. ITSC, Maui, HI, United States, pp. 2118–2125. http://dx.doi.org/10.1109/itsc.2018.8569552.

Li, L., Chen, X., 2017. Vehicle headway modeling and its inferences in macroscopic/microscopic traffic flow theory: A survey. Transp. Res. C 76, 170–188. http://dx.doi.org/10.1016/j.trc.2017.01.007.

Li, G., Jiao, Y., Knoop, V.L., Calvert, S.C., van Lint, J.W.C., 2023. Large car-following data based on lyft level-5 open dataset: Following autonomous vehicles vs. Human-driven vehicles. In: IEEE 26th International Conference on Intelligent Transportation Systems. ITSC, Bilbao, Spain, pp. 5818–5823. http://dx.doi.org/10.1109/ITSC57777.2023.10422574.

Litman, T., 2015. Autonomous vehicle implementation predictions: Implications for transport planning. In: Transportation Research Board 94th Annual Meeting. Washington D.C., United States.

Liu, S., Zheng, K., Zhao, L., Fan, P., 2020. A driving intention prediction method based on hidden Markov model for autonomous driving. Comput. Commun. 157, 143–149. http://dx.doi.org/10.1016/j.comcom.2020.04.021.

Mahdinia, I., Mohammadnazar, A., Arvin, R., Khattak, A.J., 2021. Integration of automated vehicles in mixed traffic: Evaluating changes in performance of following human-driven vehicles. Accid. Anal. Prev. 152, 106006. http://dx.doi.org/10.1016/j.aap.2021.106006.

Makridis, M., Leclercq, L., Mattas, K., Ciuffo, B., 2020a. The impact of driving homogeneity due to automation and cooperation of vehicles on uphill freeway sections. Eur. Transp. Res. Rev. 12 (1), http://dx.doi.org/10.1186/s12544-020-00407-9.

Makridis, M., Mattas, K., Ciuffo, B., 2020b. Response time and time headway of an adaptive cruise control. An empirical characterization and potential impacts on road capacity. IEEE Trans. Intell. Transp. Syst. 21 (4), 1677–1686. http://dx.doi.org/10.1109/tits.2019.2948646.

Malinin, A., Band, N., Ganshin, Alexander, Chesnokov, G., Gal, Y., Gales, M.J.F., Noskov, A., Ploskonosov, A., Prokhorenkova, L., Provilkov, I., Raina, V., Raina, V., Roginskiy, Denis, Shmatova, M., Tigas, P., Yangel, B., 2022. Shifts: A dataset of real distributional shift across multiple large-scale tasks. http://dx.doi.org/10.48550/arxiv.2107.07455, arXiv.

Meyer, J., Becker, H., Bösch, P.M., Axhausen, K.W., 2017. Autonomous vehicles: The next jump in accessibilities? Res. Transp. Econ. 62, 80–91. http://dx.doi.org/10.1016/j.retrec.2017.03.005.

Mozaffari, S., Al-Jarrah, O.Y., Dianati, M., Jennings, P., Mouzakitis, A., 2022. Deep learning-based vehicle behavior prediction for autonomous driving applications: A review. IEEE Trans. Intell. Transp. Syst. 23 (1), 33–47. http://dx.doi.org/10.1109/tits.2020.3012034.

Newell, G., 2002. A simplified car-following theory: A lower order model. Transp. Res. B 36 (3), 195–205. http://dx.doi.org/10.1016/s0191-2615(00)00044-8.

Nikitas, A., Njoya, E.T., Dani, S., 2019. Examining the myths of connected and autonomous vehicles: Analysing the pathway to a driverless mobility paradigm. Int. J. Automot. Technol. Manag. 19, 10–30. http://dx.doi.org/10.1504/ijatm.2019.098513.

Qian, R., Lai, X., Li, X., 2022. 3D object detection for autonomous driving: A survey. Pattern Recognit. 130, 108796. http://dx.doi.org/10.1016/j.patcog.2022.108796.

Rahmati, Y., Hosseini, M.K., Talebpour, A., Swain, B., Nelson, C., 2019. Influence of autonomous vehicles on car-following behavior of human drivers. Transp. Res. Rec. 2673 (12), 367–379. http://dx.doi.org/10.1177/0361198119862628.

Vieira da Rocha, T., Leclercq, L., Montanino, M., Parzani, C., Punzo, V., Ciuffo, B., Villegas, D., 2015. Does traffic-related calibration of car-following models provide accurate estimations of vehicle emissions? Transp. Res. Part D: Transp. Environ. 34, 267–280. http://dx.doi.org/10.1016/j.trd.2014.11.006.

Sak, H., Senior, A., Beaufays, F., 2014. Long short-term memory based recurrent neural network architectures for large vocabulary speech recognition. http://dx.doi.org/10.48550/arXiv.1402.1128, arXiv.

Schakel, W.J., van Arem, B., 2014. Improving traffic flow efficiency by in-car advice on lane, speed, and headway. IEEE Trans. Intell. Transp. Syst. 15 (4), 1597–1606. http://dx.doi.org/10.1109/tits.2014.2303577.

Schieben, A., Wilbrink, M., Kettwich, C., Madigan, R., Louw, T., Merat, N., 2018. Designing the interaction of automated vehicles with other traffic participants: Design considerations based on human needs and expectations. Cogn., Technol. Work 21 (1), 69–85. http://dx.doi.org/10.1007/s10111-018-0521-z.

Schwarting, W., Pierson, A., Alonso-Mora, J., Karaman, S., Rus, D., 2019. Social behavior for autonomous vehicles. Proc. Natl. Acad. Sci. USA 116 (50), 2492–24978. http://dx.doi.org/10.1073/pnas.1820676116.

Sharma, A., Zheng, Z., Bhaskar, A., 2018. A pattern recognition algorithm for assessing trajectory completeness. Transp. Res. C 96, 432–457. http://dx.doi.org/10.1016/j.trc.2018.09.027.

Sharma, A., Zheng, Z., Bhaskar, A., 2019. Is more always better? The impact of vehicular trajectory completeness on car-following model calibration and validation. Transp. Res. B 120, 49–75. http://dx.doi.org/10.1016/j.trb.2018.12.016.

Shi, X., Li, X., 2021. Constructing a fundamental diagram for traffic flow with automated vehicles: Methodology and demonstration. Transp. Res. B 150, 279–292. http://dx.doi.org/10.1016/j.trb.2021.06.011.

Siebinga, O., Zgonnikov, A., Abbink, D., 2022. A human factors approach to validating driver models for interaction-aware automated vehicles. ACM Trans. Human-Robot Interact. 11 (4), 1–21. http://dx.doi.org/10.1145/3538705.

Soni, S., Reddy, N., Tsapi, A., van Arem, B., Farah, H., 2022. Behavioral adaptations of human drivers interacting with automated vehicles. Transp. Res. Part F: Traffic Psychol. Behav. 86, 48–64. http://dx.doi.org/10.1016/j.trf.2022.02.002.

Sun, P., Kretzschmar, H., Dotiwalla, X., Chouard, A., Patnaik, V., Tsui, P., Guo, J., Zhou, Y., Chai, Y., Caine, B., Vasudevan, V., Han, W., Ngiam, J., Zhao, H., Timofeev, A., Ettinger, S., Krivokon, M., Gao, A., Joshi, A., Zhang, Y., Shlens, J., Chen, Z., Anguelov, D., 2020. Scalability in perception for autonomous driving: Waymo open dataset. In: Proceedings of the IEEE/CVF Conference on Computer Vision and Pattern Recognition. CVPR.

Teramoto, W., Honda, K., Furuta, K., Sekiyama, K., 2017. Visuotactile interaction even in far sagittal space in older adults with decreased gait and balance functions. Exp. Brain Res. 235 (8), 2391–2405. http://dx.doi.org/10.1007/s00221-017-4975-7.

Treiber, M., Hennecke, A., Helbing, D., 2000. Congested traffic states in empirical observations and microscopic simulations. Phys. Rev. E 62 (2), 1805–1824. http://dx.doi.org/10.1103/physreve.62.1805.

Treiber, M., Kesting, A., 2013a. Traffic Flow Dynamics. Springer Berlin Heidelberg, pp. 303–338. http://dx.doi.org/10.1007/978-3-642-32460-4_16, Chap. Calibration and Validation.

Treiber, M., Kesting, A., 2013b. Microscopic calibration and validation of car-following models – A systematic approach. Procedia - Soc. Behav. Sci. 80, 922–939. http://dx.doi.org/10.1016/j.sbspro.2013.05.050.

U.S. Department of Transportation – FHWA, 2008. NGSIM – Next generation simulation. http://www.ngsim.fhwa.dot.gov/. (Accessed: 2023-11-07).

van Erp, P.B., Knoop, V.L., Hoogendoorn, S.P., 2018. Macroscopic traffic state estimation using relative flows from stationary and moving observers. Transp. Res. B 114, 281–299. http://dx.doi.org/10.1016/j.trb.2018.06.005.

Vogel, K., 2003. A comparison of headway and time to collision as safety indicators. Accid. Anal. Prev. 35 (3), 427–433. http://dx.doi.org/10.1016/s0001-4575(02)00022-2.

Wang, Y., Farah, H., Yu, R., Qiu, S., van Arem, B., 2023. Characterizing behavioral differences of autonomous vehicles and human-driven vehicles at signalized intersections based on Waymo open dataset. Transp. Res. Rec. 036119812311657. http://dx.doi.org/10.1177/03611981231165783.

Wang, W., Wang, L., Zhang, C., Liu, C., Sun, L., 2022. Social interactions for autonomous driving: A review and perspectives. Found. Trends Robot. 10 (3–4), 198–376. http://dx.doi.org/10.1561/2300000078.

Wen, X., Cui, Z., Jian, S., 2022. Characterizing car-following behaviors of human drivers when following automated vehicles using the real-world dataset. Accid. Anal. Prev. 172, 106689. http://dx.doi.org/10.1016/j.aap.2022.106689.

Wilson, B., Qi, W., Agarwal, T., Lambert, J., Singh, J., Khandelwal, S., Pan, B., Kumar, R., Hartnett, A., Pontes, J.K., Ramanan, D., Carr, P., Hays, J., 2023. Argoverse 2: Next generation datasets for self-driving perception and forecasting. http://dx.doi.org/10.48550/arxiv.2301.00493, arXiv.

Xia, Y., Qu, Z., Sun, Z., Li, Z., 2021. A human-like model to understand surrounding vehicles' lane changing intentions for autonomous driving. IEEE Trans. Veh. Technol. 70 (5), 4178–4189. http://dx.doi.org/10.1109/tvt.2021.3073407.

Yao, Z., Hu, R., Jiang, Y., Xu, T., 2020. Stability and safety evaluation of mixed traffic flow with connected automated vehicles on expressways. J. Saf. Res. 75, 262–274. http://dx.doi.org/10.1016/j.jsr.2020.09.012.

Yu, H., Jiang, R., He, Z., Zheng, Z., Li, L., Liu, R., Chen, X., 2021. Automated vehicle-involved traffic flow studies: A survey of assumptions, models, speculations, and perspectives. Transp. Res. C 127, 103101. http://dx.doi.org/10.1016/j.trc.2021.103101.

Zhang, T., Jin, P.J., McQuade, S.T., Piccoli, B., 2023. Car-following models: A multidisciplinary review. http://dx.doi.org/10.48550/arxiv.2304.07143, arXiv.

Zhang, C., Sun, L., 2024. Bayesian calibration of the intelligent driver model. IEEE Trans. Intell. Transp. Syst. 1–13. http://dx.doi.org/10.1109/TITS.2024.3354102.

Zhang, Y., Talebpour, A., 2023. Characterizing human–automated vehicle interactions: An investigation into car-following behavior. Transp. Res. Rec. http://dx.doi.org/10.1177/03611981231192999.

Zhao, X., Wang, Z., Xu, Z., Wang, Y., Li, X., Qu, X., 2020. Field experiments on longitudinal characteristics of human driver behavior following an autonomous vehicle. Transp. Res. C 114, 205–224. http://dx.doi.org/10.1016/j.trc.2020.02.018.

Zheng, F., Liu, C., Liu, X., Jabari, S.E., Lu, L., 2020. Analyzing the impact of automated vehicles on uncertainty and stability of the mixed traffic flow. Transp. Res. C 112, 203–219. http://dx.doi.org/10.1016/j.trc.2020.01.017.